



# BER and throughput performances of IEEE 802.11ay SC-PHY over measured 60 GHz indoor channels

Ladislav Polak<sup>1</sup> · Jiri Milos<sup>1</sup> · Radim Zedka<sup>1</sup> · Jiri Blumenstein<sup>1</sup> · Christoph Mecklenbräuer<sup>2</sup>

Accepted: 30 May 2022 / Published online: 26 June 2022

© The Author(s), under exclusive licence to Springer Science+Business Media, LLC, part of Springer Nature 2022

## Abstract

The IEEE 802.11ay is an emerging system that will become a full member of the big family of the IEEE 802.11 standards in the near future. Compared to its predecessor IEEE 802.11ad, it promises to offer higher system flexibility and more reliable wireless communication links for short distances in millimeter-wave bands. This paper provides a simulation-based performance study of IEEE 802.11ay single carrier-physical (SC-PHY) layer for different transmission modes and scenarios. For this purpose, a MATLAB-based IEEE 802.11ay SC-PHY simulator is introduced. Next, 60 GHz indoor channel models based on extensive real-world indoor measurements, conducted by ourselves, are created and used to analyze the performance of IEEE 802.11ay SC-PHY in terms of Bit Error Ratio and data throughput. Both the simulator and channel models are available online. A phase noise behavioral model to emulate channel impairments is also considered and used in this work. The obtained results show how the IEEE 802.11ay SC-PHY system employing different transmission modes is influenced under various channel conditions.

**Keywords** 60 GHz indoor channel model · IEEE 802.11ay · phase noise · PHY-level simulation · RF measurement · WLAN

## 1 Introduction

Wireless Local Area Networks (WLANs) can employ different IEEE 802.11 technologies [1] to realize a wireless communication link in a wide range of licensed or unlicensed (Industrial Scientific Medical—ISM) radio frequency (RF) bands. Effective utilization of the RF spectrum and flexible system configurations are among the main requirements on the fifth generation (5G) networks [2,3]. Therefore, in the last decade, the already big family of the IEEE 802.11 standards has been extended with several new members. Standards,<sup>1</sup> like IEEE 802.11ah/af/ad/ay, can ensure reliable data transmission in a wide range of the RF spectrum (from sub-1 GHz up to 60 GHz).

The IEEE 802.11ay standard,<sup>2</sup> as the successor of IEEE 802.11ad [4], was approved in March 2021. With focus on the license-free millimeter-waves (mm-Waves) of the RF spectrum, it was developed to create a short-range (in terms of several hundreds of meters) 60 GHz wireless link mainly in an indoor environment. Thanks to the support of different physical (PHY) layer specifications, multiple-input multiple-output (MIMO) schemes, and advanced techniques to achieve wider channel bandwidths (channel bonding and aggregation) [5], theoretically, it is possible to achieve a data rate around 40 Gbps (a link-rate per stream) and a transmission distance of  $\approx 300$  m. Thereby, the 802.11ay system will be suitable for transmitting or streaming data hungry multimedia content (e.g. videos in Ultra High Definition (UHD) [6]) in an indoor environment for short distances.

Three PHY specifications [7], also called PHY modes, are defined in the IEEE 802.11ay standard: control (C-PHY), Single Carrier (SC-PHY) and Orthogonal Frequency Division Multiplexing (OFDM-PHY). These PHY-modes, except for C-PHY, support a wide range of modulation coding schemes (MCSs) to provide different application-specific functions of 802.11ay [8,9]. Therefore, the IEEE 802.11ay

<sup>1</sup> In this work, expressions "IEEE 802.11 standard" and "IEEE 802.11 technology" are interchangeable.

✉ Ladislav Polak  
polakl@vut.cz

<sup>1</sup> Department of Radio Electronics, Faculty of Electrical Engineering and Communications, Brno University of Technology, Technicka 12, 616 00 Brno, Czech Republic

<sup>2</sup> Institute of Telecommunications, TU Wien, Vienna, Austria

<sup>2</sup> In this work, shorter expression "802.11ay" is also used.

system excels with high configuration flexibility allowing to employ it in different use cases (e.g., wireless transmission of an uncompressed UHD video, high speed data transfer or wireless connection of devices with different peripherals) [7]. This paper is focused on the SC-PHY layer of the IEEE 802.11ay standard.

## 1.1 Related work

In previous years, mainly the predecessor of 802.11ay system, namely 802.11ad, was in the spotlight of research. Different simulation and measurement-based works [10–15] have dealt on the performance and features of 802.11ad. Their outputs revealed that the requirements on signal-to-noise ratio (SNR) to achieve the target bit error ratio (BER) in SC and OFDM-PHY schemes [10–12] are different. Next, it was observed that the performance of 802.11ad-based mm-Wave links highly depends on the used antenna configuration, non- and line-of-sight (NLOS and LOS) conditions and indoor environment characteristics (e.g. sensitivity to blockage caused by device and human motions) [13–15].

In recent years, only a few of works have focused on the performance study of the 802.11ay-based wireless link. In 2018, da Silva et al. [16] presented a pioneering simulation-based analysis of the 802.11ay SC-PHY system in terms of peak-to-average-power ratio (PAPR) and frame error ratio (FER). It was stated that the 802.11ay system has several technical advancements on the PHY level, e.g. new frame format or enhanced beamforming training. In [17], the BER performance of selected MCSs of 802.11ay signal under Additive White Gaussian Noise (AWGN) and Quasi-Deterministic (Q-D) channel conditions is evaluated in terms of different effective SNR metric schemes. It was shown that the considered metrics differ in implementation complexity and their performance is also depending on the used PHY mode.

Lei and at al. [18] build an ns-3 based simulation platform on a system level for analysing an 802.11ay-based communication link employing channel bonding. The performance analysis of the 802.11ay-based wireless link, created in a conference room, showed high data throughput when a single channel bonding technique is used. Similar study focusing on the maximum achievable throughput for the 802.11ay system has been presented in [19]. Simulations were provided in a channel model with strong nature of LOS communication. The obtained results confirmed theoretical assumptions, i.e. the higher is the number of bounded channels, the higher is the achievable data throughput.

The 60 GHz channel characteristics and their influence on a short-range 802.11ay signal, generated for selected MCSs, were studied in [20–23]. Results showed that the 802.11ay signal using M-QAM modulation with low M-order has similar resistance against noise in channels with LOS and NLOS

conditions. Authors of the work [21] emphasized that new use cases for IEEE 802.11ay will lead to new channel model creations.

Nowadays, research activities around IEEE 802.11ay, as it was mentioned in [18], are focused on two main fields. First, there is an effort to analyse and improve the media access control (MAC) layer protocol and related algorithms [5,7]. Second, attention is devoted to the PHY layer including the performance study of the 802.11ay PHY specifications for different transmission scenarios, the improvement of the signal processing chain [7] and the design and development of functional blocks for TX/RX [24].

From the above presented brief overview we can conclude the following:

1. Performance study of 802.11ay SC-PHY focusing on the connection between different system configuration and transmission modes over measured 60 GHz indoor channels is not reported so far and,
2. Publicly available measurement-based 60 GHz indoor channel models for simulation-based 802.11ay performance study are not widely available.

## 1.2 Contribution

The main contributions of our paper are summarized as follows:

1. We provide performance study of 802.11ay SC-PHY over 60 GHz indoor channel models in terms of BER and data throughput. Our study also includes exploring of the influence of RF impairments, caused by phase noise (PN), on the 802.11ay SC-PHY based signal operating in the mm-Wave band.
2. We introduce a MATLAB-based IEEE 802.11ay SC-PHY baseband simulator with a set of settable system parameters and with a support of different transmission modes. It allows to provide 802.11ay SC-PHY performance studies in terms of BER, FER and throughput and excels with stable reproducibility. Next, a PN behavioral model to emulate RF impairments is also implemented in the simulator. For future research purposes, the simulator is publicly available under the MIT License for download from GitHub.<sup>3</sup>
3. We present 60 GHz indoor channel models for performance studies of the 802.11ay system in our simulator. There is available channel model for SISO scheme [12] as well as for receive diversity (SIMO –  $1 \times 2$ ) and spatial multiplexing (MIMO –  $2 \times 2$ ) schemes. All channel models are based on the dataset obtained from measurements in an indoor office. The 60 GHz indoor channel

<sup>3</sup> <https://github.com/jirimos/802.11ay-phy-sim>.

measurement campaigns are described in detail. To promote reproducibility of our research, the measured dataset is also publicly available.

### 1.3 Organization

This paper is organized as follows. After the Introduction, in Sect. 2, the created IEEE 802.11ay SC-PHY MATLAB simulator is introduced. The used measurement testbed and the 60 GHz indoor measurement campaigns conducted to obtain 60 GHz channel models are described in Sect. 3. Simulation-based performance studies of 802.11ay SC-PHY are evaluated in Sect. 4. Finally, Sect. 5 concludes this paper.

## 2 The IEEE 802.11ay SC-PHY baseband MATLAB simulator

This section introduces the basic structure of the created IEEE 802.11ay SC-PHY MATLAB simulator. Some basic functional blocks (e.g., scrambler) of this simulator were created in our previously introduced simulators [12,25,26]. These functional blocks were re-used in this simulator and modified to meet requirements for the 802.11ay SC-PHY signal processing chain. Control System, Signal Process-

ing, DSP System and Communications System toolboxes are required to run the simulator.

### 2.1 wifi\_sim\_batch

The overall structure (scripts and functions) of the IEEE 802.11ay SC-PHY MATLAB simulator and the baseband signal processing chain in TX are shown in Fig. 1. The simulator is launched via batch file *wifi\_sim\_batch.m* only. The batch file contains a set of parameters to control the whole simulation including the load of the 802.11ay SC-PHY system parameters (*load\_wifi\_params.m*). It is possible to simulate data transmission for a single user (SU) on the level of either individual MCSs or for a complete set of MCSs in a loop. In terms of the configuration of MCSs in IEEE 802.11ay, the SC-PHY scheme, compared to C-PHY and OFDM-PHY, enables to achieve the best trade-off between implementation complexity and spectral efficiency. This PHY specification for 802.11ay, including identification of control mode, allows to select among 21 different MCSs [9].

Parameters like the range of SNR values, the number of frames per SNR and the number of user data octets (*LENGTH*) can also be defined in the batch file. The optional system parameters are listed in Table 1. After starting the simulation, the settings are checked (*mcs\_definition.m*) and the



**Fig. 1** Scripts and functions of the IEEE 802.11ay SC-PHY MATLAB simulator; [right] baseband signal processing chain in the IEEE 802.11ay SC-PHY transmitter (TX)

**Table 1** Overview of optional system parameters in the file "wifi\_sim\_batch.m" of the IEEE 802.11ay SC-PHY simulator

System parameter	Possible values	Description
antMode	'SISO', 'Rx/D' or 'MIMO'	Antenna mode
TxRxAnt	11, 12 or 22	Number of transmitting and receiving antennas
useNUC	true or false	Non-uniform constellations (only for MCS 17 to MCS 21)*
use8PSK	true or false	$\pi/2$ -8PSK constellation in MCS 12 and MCS 13
GuardInterval	'short', 'normal' or 'long'	The length of guard interval
LDPCMatrix	'normal' or 'lifted'	LDPC matrix with normal or extended (lifted) size

\*Available only for AWGN and 60 GHz SISO channel models

simulation parameters are stored in the file *wifi\_params.m*. Parameters and data which should be saved after the simulation for further analysis can be defined in the file *result\_allocation()*. The main simulation takes place in *sim\_file.m*. This file contains a loop for sweeping SNR values and the number of 802.11ay frames used in simulations. It also informs the user about the current simulation being run.

## 2.2 WIFI\_TX\_ay()

The function *WIFI\_TX\_ay()* contains the whole TX model of the 802.11ay SC-PHY system. The input of this function is the m-function *load\_wifi\_params* used for load Wi-Fi parameters for simulation. The PHY layer service data unit (PSDU) and PSDU padding are generated randomly according to MCS and *LENGTH*. The number of PSDU padding bits is calculated as follows:

$$N_{\text{DATA\_PAD}} = \left( N_{\text{CW}} L_{\text{CW}} \frac{R}{\rho} \right) - \text{LENGTH} \cdot 8, \quad (1)$$

where  $N_{\text{CW}}$  is the total number of low-density parity-check (LDPC) codewords for a single user,  $L_{\text{CW}}$  is the LDPC codeword length in bits, which is usually equal to 672 (normal LDPC matrix) or 1344 (lifted LDPC matrix) [27,28],  $R$  marks the code rate (CR) and  $\rho$  is the repetition factor (see Sect. 4). The value of  $N_{\text{CW}}$  is given as:

$$N_{\text{CW}} = \left\lceil \frac{\text{LENGTH} \cdot 8}{L_{\text{CW}} \frac{R}{\rho}} \right\rceil. \quad (2)$$

The generation of input data is followed by the process of scrambling to break up long sequences of zeros and ones. For this purpose, a linear feedback shift register with a generator polynomial is used [9]. The scrambling of the padded PSDU bits is provided by function *txScrambling()*.

In the next step, the forward error correction (FEC) of the data is ensured on the level of LDPC encoding. LDPC encoding is performed in the script *ayLDPCEncoding()*, partly employing built-in MATLAB functions.

In terms of CR, the FEC process can have five levels:  $CR = \{1/2, 5/8, 3/4, 13/16, 7/8\}$ . It is important to note two things. Firstly, the information bits are repeated (not the parity bits) only for one MCS (see Sect. 4). Secondly, CR of 2/3 and 5/6 can also be used for 8-PSK modulation.

According to the defined MCSs for the IEEE 802.11ay SC-PHY, the  $\pi/2$ -{BPSK, QPSK, 16-QAM and 64-QAM} uniform constellation schemes can be used to modulate the FEC encoded data. Additionally,  $\pi/2$ -8-PSK modulation and non-uniform constellation of  $\pi/2$ -64-QAM, marked as NUC [16], are also supported. The encoded bits are led into the function *ayModulator()* that provides mapping to complex-valued symbols according to the selected MCSs and system parameters *use8PSK* and *useNUC* (see Table 1). It uses a built-in MATLAB function for rectangular modulations with a custom-built  $\pi/2$  rotation. The rectangular constellations are normalized to unit of power. The NUC for MCSs 17-21 are shown in Fig. 2. In the next step, the constellation symbols are divided into SC symbol blocks [16]. For constellations with 64 points ( $\pi/2$ -64-QAM and NUC of  $\pi/2$ -64-QAM), a block-based interleaver is applied to perform interleaving inside the single carrier symbol block [29].

In the case of another transmission scheme than SISO, signal processing continues by the block space-time block code (STBC) employed for mapping of the  $N_{\text{SS}}$  constellation symbols into  $N_{\text{STS}}$  space-time streams. For  $N_{\text{STS}} > 1$ , direct mapping is used. According to [29], the 802.11ay SC-PHY mode uses a single STBC scheme with  $N_{\text{STS}} = 2$ . Al-Dhahir's STBC [30] is implemented and employed in our simulator, because it provides diversity gain, minimum block delay and full code-rate to broadband systems based

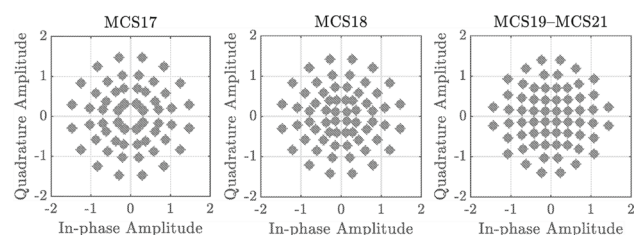


**Fig. 2** The NUC constellations for MCSs 17-21



on a single carrier scheme combined with frequency domain equalization (SC-FDE). It also allows to extend original narrowband Alamouti's STBC into broadband SC-FDE systems with two transmit paths.

In the next stage, namely in the function *ayBlockingAndGI()*, the SC symbol blocks are split into blocks with a length of 448. Between these blocks other symbols, so called Golay guard sequences, are inserted and modulated with  $\pi/2$ -BPSK. They serve as pilots and can also be used for equalization (at the RX side) in the frequency domain [7,9,31,32]. The guard interval (GI) consists of a Golay complementary function, labeled as Ga<sub>32</sub>, Ga<sub>64</sub> or Ga<sub>128</sub>. Symbols Ga<sub>32</sub>, Ga<sub>64</sub> and Ga<sub>128</sub> mark GI with a short, normal and long length (see Table 1), respectively. The GI is pre-pended to each block of SC symbols. The function *ayBlockingAndGI()* also generates a preamble for legacy-short training and legacy-channel estimation fields (L-STF and L-CTF) [16]. After that, the 802.11ay SC-PHY baseband signal is created.

The 802.11ay SC-PHY baseband signal is the input of function *channel()*. This function allows the user to provide a performance study of 802.11ay SC-PHY data transmission under different channel models and impairments. The created IEEE 802.11ay SC-PHY simulator offers three basic types of channel models to emulate different transmission conditions: Additive White Gaussian Noise (AWGN), user defined and real-world 60 GHz indoor channel models. The AWGN channel model, employing the *awgn* in-built MATLAB function, is recommended to be used for the 802.11ay SC-PHY performance study on reference level. The channel model labeled as "user defined" allows the user to define the basic parameters of a custom fading channel model (the number of taps, delay and power level) [33]. Finally, real-world 60 GHz indoor channel models can be used in the simulations. A dataset for real-world channel models was obtained from an indoor office measurement campaign conducted at BUT, Department of Radio Electronics (DREL). The data are stored in *mat* files and can be easily employed in MATLAB. It serves as a database-oriented channel model from which individual channel realizations are loaded. Channel impulse responses (CIRs) and channel transfer functions (CTFs) of a time invariant indoor channel with a 10 GHz bandwidth spanning the frequencies from 55 to 65 GHz are provided.

Our 802.11ay SC-PHY simulator also allows to study the influence of RF channel impairments. For this purpose, according to [34], a PN behavioral model is utilized. In general, the influence of PN on the 60 GHz-based wireless communication link is not negligible, especially on the level of its BER performance and synchronization problems. In the simulator, the phase-locked loop (PLL) output phase

noise is modeled as a one-pole and one-zero model. It can be described as [35]:

$$\text{PSD}(f) = \text{PSD}(0) \left[ \frac{1 + \left(\frac{f}{f_z}\right)^2}{1 + \left(\frac{f}{f_p}\right)^2} \right], \quad (3)$$

where PSD(0) denotes the low frequency phase noise below the loop-filter bandwidth of the PLL [36],  $f_z$  and  $f_p$  mark zero and pole frequency, respectively. In the considered PN model (on the level of time-domain), PSD(0) = -90 dBc/Hz,  $f_p = 1$  MHz and  $f_z = 100$  MHz are considered. The PSD at infinite frequency has a value of -130 dBc/Hz.

### 2.3 WIFI\_RX\_ay()

The IEEE 802.11ay frame, influenced by the channel model, leads to function *WIFI\_RX\_ay()*. Firstly, the preamble and user data samples are separated (*parseFrame()*). The preamble samples are used for synchronization and channel estimation. The user data samples are processed within the function *ayRXDataField()*. This function contains additional sub-functions like deblocking, demodulation, LDPC decoding and descrambling, which in comparison with TX provide inverse signal processing. The extracted PSDU, determined by function *extract\_PSDU()*, is compared with known PSDU (TX) and the numbers of erroneous bits and frames are calculated for each repetition given by the number of transmitted frames per SNR value. It is done in function *result\_calculation()*. Finally, the obtained results are stored. Function *load\_filename()* enables the user to load the saved results and use them for further purposes (e.g., visual representation).

### 2.4 Notes: equalization

Channel estimation in a wideband communication system is vital. Predefined sequences, already known to the RX, are transmitted over the channel. In the RX, these sequences are evaluated and used to estimate the channel. In 802.11ay SC-PHY, complementary Golay sequences are used for this purpose [31]. In the created simulator, the Channel Estimation Field (CEF) [9], available in each packet, consists of the Golay sequences with a length of 128 samples (Ga<sub>128</sub>, Gb<sub>128</sub>) creating a field of 1152 samples. The complete CEF field is modulated with  $\pi/2$ -BPSK. At the RX side, it is processed with the corresponding Ga<sub>128</sub> or Gb<sub>128</sub> sequence in a correlator. The output of the correlator is averaged and the estimated CIR, labeled as  $h(t)$ , with a length of 128 samples

is obtained. More details about Golay sequences including determination of CIR can be found in [31].

### 3 Measurement setup and campaign for 60 GHz channel measurement

As far as LOS MIMO communications is concerned, it turns out that the system performance is primarily determined by the installation of TX and RX antennas and the surrounding environment. In order to have real-world channel realizations instead of often simplified channel models, a channel sounding campaign in the 55–65 GHz band was performed in an indoor environment at the Brno University of Technology. The classroom, where the measurements were conducted, is made from concrete, walls are lined with plasterboard and the ceiling material is mineral wool with paint finish. The classroom with dimensions  $10 \times 7$  m contains several tables surrounded by chairs, a desk, several wardrobes and eight operable windows (see Fig. 3). A set of tables are positioned in the middle of room while three tables are close to the windows. For next measurements a similar classroom with dimensions  $15 \text{ m} \times 6 \text{ m} \times 2.8 \text{ m}$  was used. The measurement captures two typical use cases of indoor Wi-Fi application, which we denote as measurement Scenario I and Scenario II. The difference between the stated scenarios is namely in the geometry of the measurement location (medium-size laboratory vs. small-size laboratory) and the fact that in Scenario I majority of the reflective surfaces are covered by absorbers, thus exhibiting significantly lower delay spread than in the case non-covered scenario (see Fig. 4). This way, we emulate

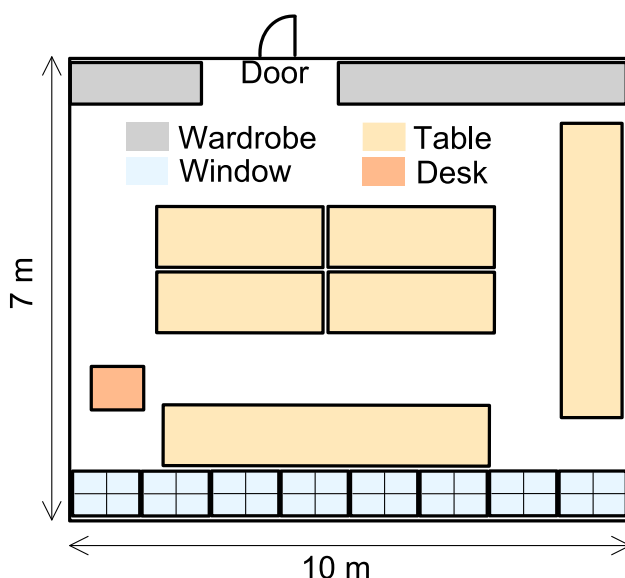


Fig. 3 Floor plan of the classroom

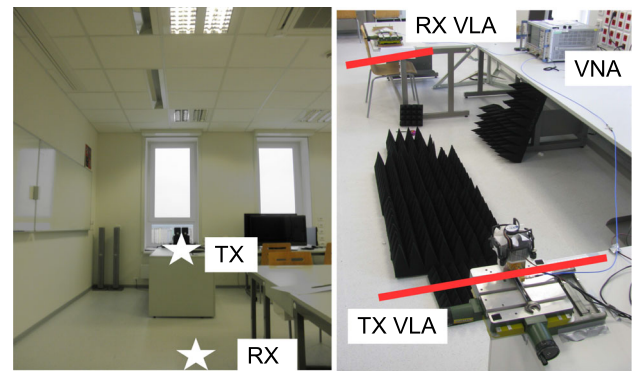


Fig. 4 The measurement site. The linear movement with the  $xy$ -tables formed a virtual linear array (VLA) both at TX and RX sides. We depict both scenarios, one padded with absorbers having lower delay spreads, the second scenario exhibits higher delay spread thanks to metallic objects in the scene

two different classes of channels, i.e. with high and low time dispersion.

#### 3.1 55–65 GHz channel sounder

The utilized frequency domain channel sounder is composed of a vector network analyzer (VNA) and a pair of TX and RX antennas. The virtual MIMO channel is measured by changing the positions of the TX and RX antennas utilizing the  $xy$ -tables (more details can be found in [37]). The channel sounder operates on the frequency domain measurement principle as demonstrated in [38] (as opposed to the time-domain principle presented for the mm-Wave band in [39]). In this method, a narrow-band sounding signal is swept from 55 to 65 GHz with a step size of 10 MHz.

The R&S ZVA67 four-port VNA is utilized to measure the transmission coefficient between TX and RX antennas. The dynamic range is extended with power amplifier (QuinStar QPW-50662330), which has a measured gain of 35 dB in the band of interest. We use two WR15 open-ended waveguides as TX and RX antennas with the radiation pattern as depicted in Fig. 5 [40]. Phase-stable coaxial cables are used to avoid

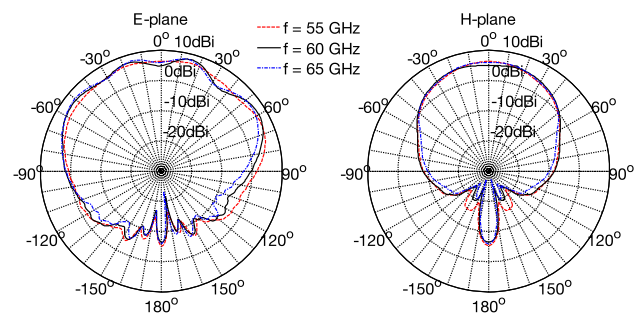


Fig. 5 Measured gain pattern of the open-ended waveguide antennas in the E- and H-planes

the degradation of the measured phase due to mutual movements of the TX and RX antennas. A VNA output power of 5 dBm and IF bandwidth of 100Hz are used. The system’s dynamic range is approximately 50dB. Before the channel sounding, a full 4-port calibration process was performed.

### 3.2 Data acquisition and post processing

Due to the fact that the measurement environment does not contain any moving objects, the measured channel is time invariant and the measured frequency domain CTF is given by:

$$\tilde{h}_{ji}(f) = s_{ji}^{21}(f), \tag{4}$$

where  $f$  denotes the measurement frequencies,  $i, j$  are the spatial indices of the elements of the virtual TX, RX uniform linear array (ULA), and  $s^{21}$  is the scattering parameter, which represents the transmission from the feed of the TX antenna to the output of the RX antenna. By Inverse Fourier Transform (IFT), we convert the CTF into the CIR as [37]:

$$h_{ji}(n) = \sum_{g=0}^{N-1} \tilde{h}_{ji}(f) \exp\left(j \frac{2\pi f n}{N}\right), \tag{5}$$

where  $h_{ji}(n)$  is the discrete version of the  $ji$ -th element of the multipath channel  $H$  and  $N$  is the number of measured frequency points. A sample of characteristics of the transmission channel in frequency and time domain is plotted in Figs. 6 and 7, respectively.

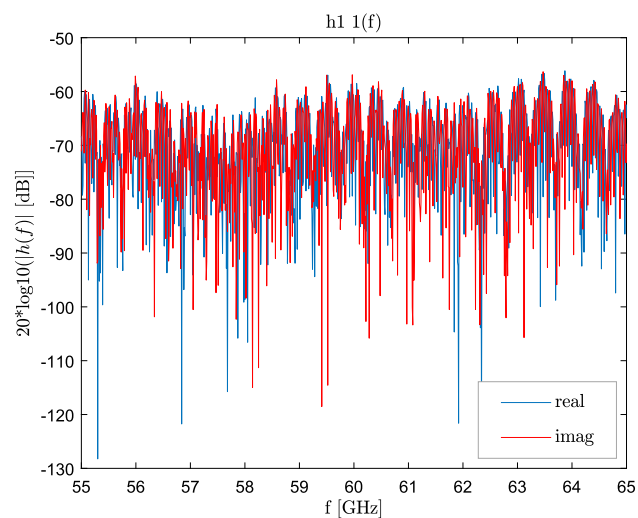


Fig. 6 Measured CTF

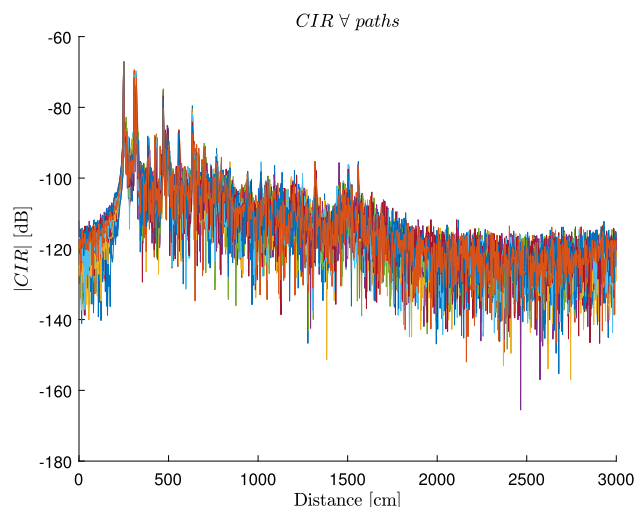


Fig. 7 CIR converted from CTF by IFT

### 3.3 Measurement scenarios

#### 3.3.1 Scenario I

Scenario I accounts for a medium-size laboratory that is shown in Fig. 4 [right]. The absorbers are used to suppress reflections from the floor (ground reflection) and metallic table legs. The purpose of using absorbers is to highlight the differences with Scenario II, where no absorbers are used. The TX–RX distance is 3 m and the height of antennas above the ground is 1.2 m.

Both the TX and RX antennas are placed on  $xy$ -tables [37] with a sub-millimeter shifting step. As depicted in Fig. 4, with proper alignment of the TX and RX  $xy$ -tables, virtual TX and RX ULA can be emulated using a single pair of antennas. In this scenario, four sets of data were measured corresponding to a  $4 \times 4$  and  $6 \times 6$  MIMO system.

#### 3.3.2 Scenario II

Scenario II represents a smaller-size laboratory environment (see Fig. 4 [left]). In this scenario, the TX–RX distance is reduced to 2.5 m. The TX–RX link is close to a wall on the left side and no absorbers are used to shield the ground and metallic table legs, thus effectively creating a scenario with significantly richer scattering.

The parameters such as the antenna height, tilt angles and measurement procedure itself are identical as those of Scenario I. Three sets of data were measured corresponding to a  $4 \times 4$  MIMO system.

Despite the use of absorbers, Scenario I can be considered to be a representative example of the channel conditions that are typically encountered in the STA-AP sub-scenario

of IEEE 802.11 WLAN [41], where the access point (AP) is installed on the ceiling and the STA (station, or communication device) is placed on a table in the same room.

In this regard, Scenario II can be viewed as an emulation of the STA-STA (device-to-device) sub-scenario of WLAN. In total, we obtained seven virtual MIMO realizations and 132 CIR for the two scenarios.

## 4 Performance of the IEEE 802.11ay SC-PHY system

In this section, with the aim to demonstrate the functionality and capabilities of our simulator, we present the outputs of simulations for some selected use cases and briefly discuss the obtained results. The BER and throughput curves for MCSs were obtained for the following system parameters: the user data octet has a length of 300, ‘lifted’ LDPC matrix is used, the length of GI is ‘normal’ and Log-Likelihood Ratio (LLR) decision is used in the LDPC decoder. The MCSs, used in the simulations, are listed in Table 2.

**Table 2** Overview of MCSs for the 802.11ay SC-PHY mode

MCS	Modulace	$N_{CBPS}^a$	Repetition	$CR^b$
1 <sup>c</sup>	$\pi/2$ -DBPSK	1	1	1/2
2	$\pi/2$ -BPSK	1	2	1/2
3	$\pi/2$ -BPSK	1	1	1/2
4	$\pi/2$ -BPSK	1	1	5/8
5	$\pi/2$ -BPSK	1	1	3/4
6	$\pi/2$ -BPSK	1	1	13/16
7	$\pi/2$ -BPSK	1	1	7/8
8	$\pi/2$ -QPSK	2	1	1/2
9	$\pi/2$ -QPSK	2	1	5/8
10	$\pi/2$ -QPSK	2	1	3/4
11	$\pi/2$ -QPSK	2	1	13/16
12	$\pi/2$ -QPSK	2	1	7/8
13	$\pi/2$ -16QAM	4	1	1/2
14	$\pi/2$ -16QAM	4	1	5/8
15	$\pi/2$ -16QAM	4	1	3/4
16	$\pi/2$ -16QAM	4	1	13/16
17	$\pi/2$ -16QAM	4	1	7/8
18	$\pi/2$ -64QAM	6	1	5/8
19	$\pi/2$ -64QAM	6	1	3/4
20	$\pi/2$ -64QAM	6	1	13/16
21	$\pi/2$ -64QAM	6	1	7/8

<sup>a</sup>Number of coded bits per symbol

<sup>b</sup>Code Rate

<sup>c</sup>This MCS is used to identify the control mode

## 4.1 AWGN channel

In this subsection, attention is devoted to the BER and data throughput curves, obtained for the AWGN channel (reference transmission scenario). We provided simulations for two transmission modes. Dependence of BER and data throughput on the values of SNR for the transmission scheme SISO is shown in Fig. 8. Curves for all MCSs are plotted (the legend, as in the remaining parts of the article, is valid for both graphs). In terms of SNR, the operating range is between  $-10$  dB and  $20$  dB. The lowest data rate, around  $0.4$  Gbps, is obtained for MCS = 1 used to identify the control mode—C-PHY) at SNR =  $-4.5$  dB. It is important to mention that the SNR is defined as the post-FFT ratio at the receiving antenna [26,42]. For MCSs from 1 to 7, BER =  $10^{-3}$  can be achieved at SNR <  $5$  dB while for MCS = 21 (CR =  $7/8$ , modulation  $\pi/2$ -64QAM), the SNR is below  $20$  dB.

The BER and data throughput performance for MIMO with scheme  $2 \times 2$  using spatial multiplexing (SM) are shown in Fig. 9. Compared to the SISO case, the positive effect of spatial multiplexing on the data throughput can be observed. For MCS = 21, the data rate [43] can be higher than  $11$  Gbps. The obtained BER curves confirm that MIMO used by a way of SM is not appropriate to ensure more robust data transmission. Such results meet with the theory. At the using of SM scheme, different data streams are transmitted from each antenna and are multiplexed in space. Consequently, the data rate is increased without any change in bandwidth or transmission power. Compared to a conventional MIMO system, its advantage is evident.

## 4.2 Real-world 60 GHz indoor channel

In this subsection, the performance of the 802.11ay SC-PHY system employing different transmission schemes in real-world 60 GHz indoor channel is in the spotlight. As was previously emphasized, IEEE 802.11ay was developed to create a wireless communication link in mm-Wave bands. Hence, investigation of its performance influenced by characteristics of a 60 GHz indoor channel model is vital. In this work, channel model obtained from measurement Scenario I (see Sect. 3.3) is used for this purpose.

Figure 10 shows the BER and data throughput performance of the 802.11ay SISO signal for different SNR values in a measured 60 GHz indoor multipath channel. According to theoretical assumptions, the 60 GHz indoor channel causes higher requirements on the 802.11ay-based wireless link resulting in higher values of SNR. However, it must be noted that lower order MCSs (up to 11), in comparison with the AWGN channel (see Fig. 8), show only a minimal increase in the values of SNR. To achieve BER =  $10^{-3}$  at



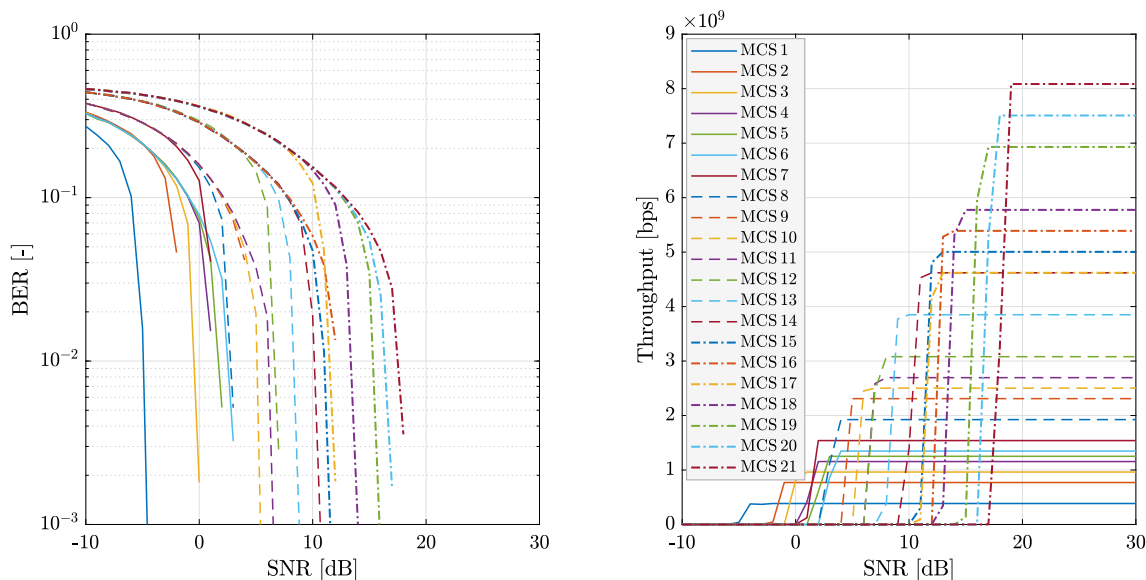


Fig. 8 BER and throughput curves of the 802.11ay SISO signal depending on SNR in the AWGN channel

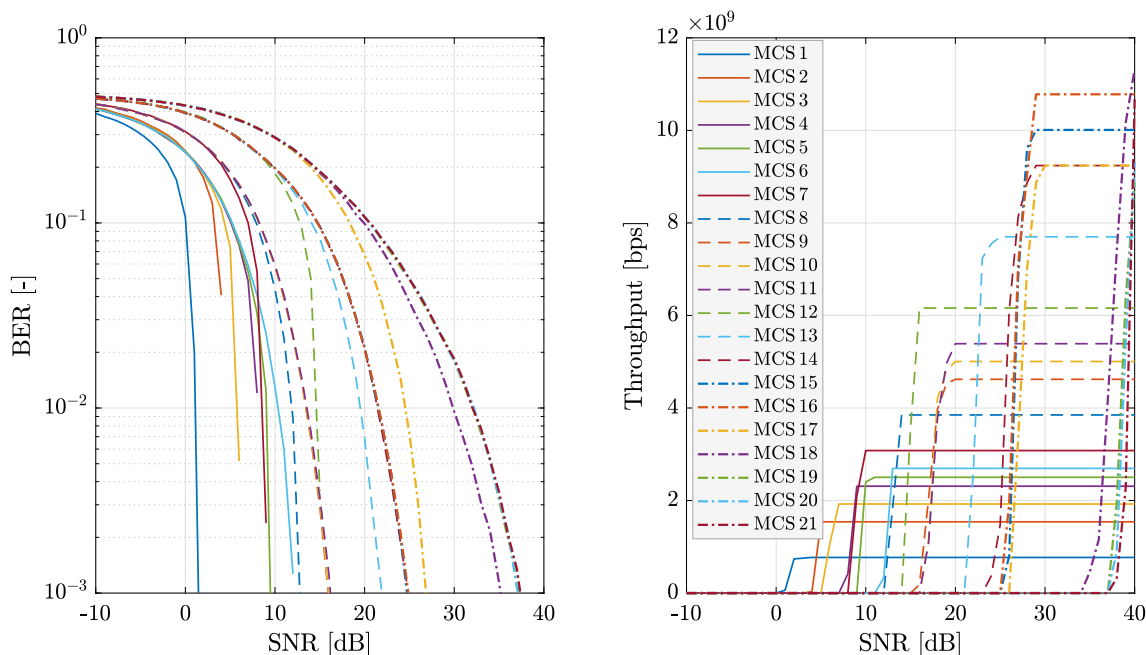
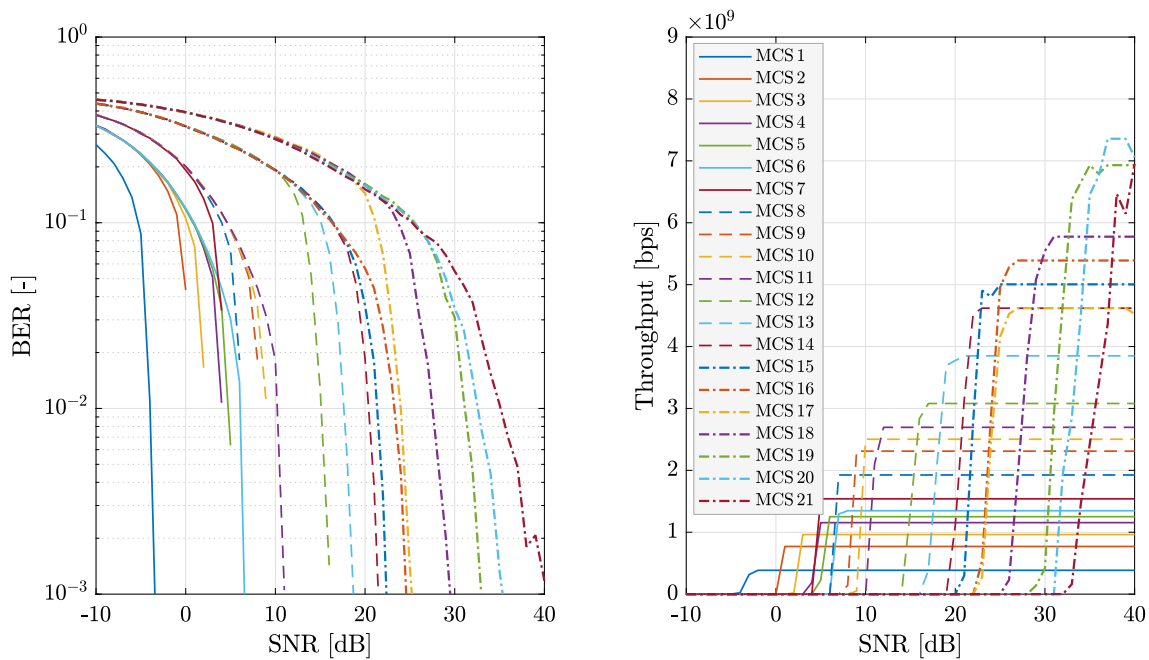


Fig. 9 BER and throughput curves of the 802.11ay MIMO (scheme 2 × 2 - spatial multiplexing) signal depending on SNR in the AWGN channel

MCS 18-21 (using  $\pi/2$ -64QAM modulation), the value of SNR must be higher than 30 dB. For MCS = 21, the data rate is around 7 Gbps.

The same performance study was provided for SIMO (scheme 1 × 2) and MIMO (scheme 2 × 2 - SM) configurations and the results are plotted in Figs. 11 and 12, respectively. The obtained BER and throughput curves show advantages of receive diversity for the 60 GHz indoor multipath channel. It is visible that the usage of SIMO scheme allows for the receiver to effectively combat the fading that

often occurs in an environment with a nature of multipath propagation. The noticeable performance degradation for the 802.11ay SC-PHY using MIMO SM, mainly for higher order MCSs, is probably caused by severe multipath effects (see Figs. 9 and 12). These results confirm that, in general, MIMO employing SM is not intended to make the data transmission robust. SM is appropriate in a case when good transmission conditions exist [44,45]. Hence, MIMO using SM for 60 GHz indoor channel with poor transmission conditions is not appropriate.



**Fig. 10** BER and throughput curves of the 802.11ay SISO signal depending on SNR in the measured 60 GHz indoor multipath channel

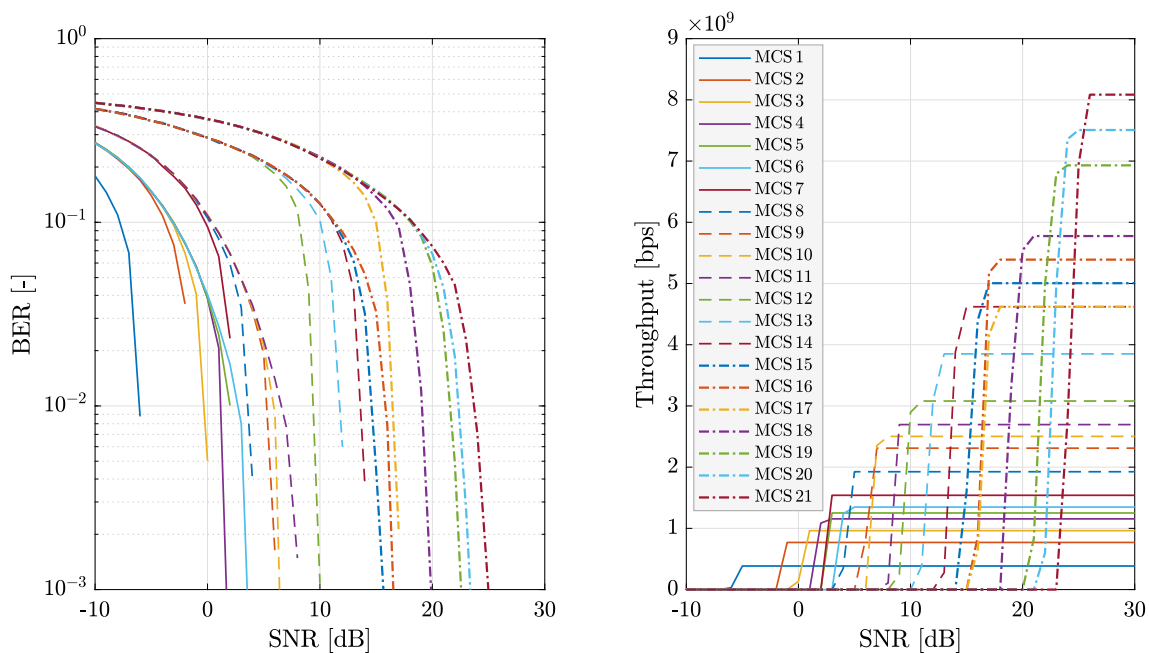


**Fig. 11** BER and throughput curves of the 802.11ay SIMO (scheme  $1 \times 2$ ) signal depending on SNR in the measured 60 GHz indoor multipath channel

### 4.3 RF impairments

Wireless systems operating in the 60 GHz bands are sensitive to RF impairments caused by phase noises (PNs) [36]. The last part of this section is focused on the immunity of the 802.11ay SC-PHY system against PNs. Attention is also devoted to NUCs and its employment in such scenarios. It

must be noted that only NUCs with 64 signal points (in the simulations MCS 18–21) are considered. In all cases, SISO configuration and AWGN and 60 GHz channel models are utilized.

Figures 13, 14 and 15 capture the outputs of simulations provided for the 802.11ay SC-PHY SISO signal in AWGN (reference) channel and 60 GHz measured channel under the

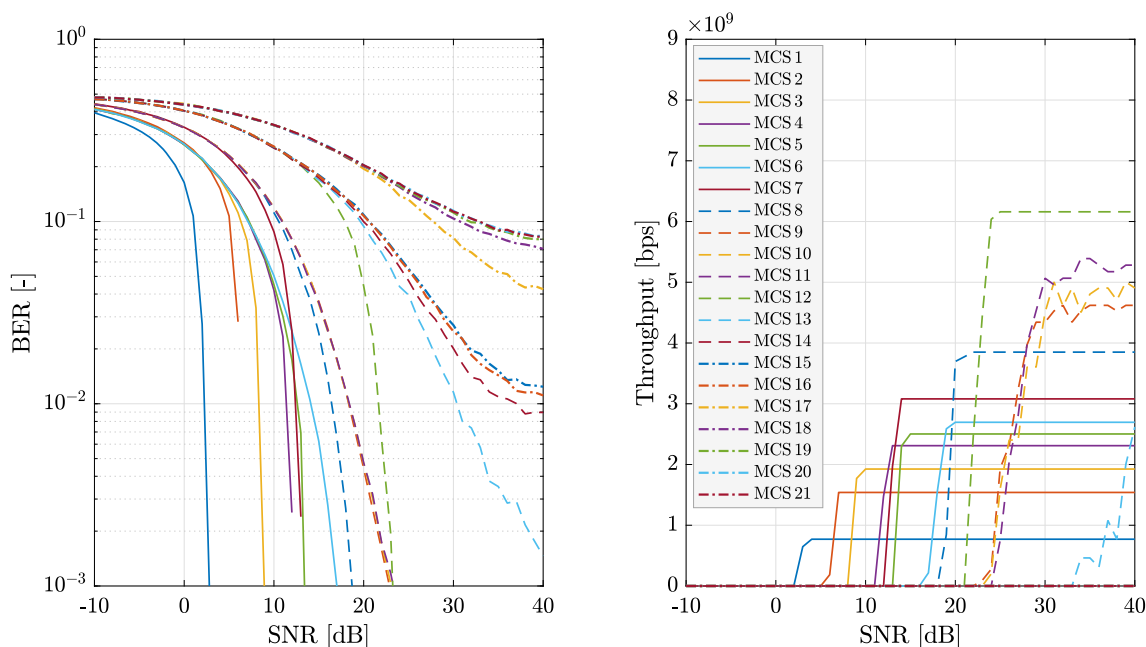


Fig. 12 BER and throughput curves of the 802.11ay MIMO (scheme  $2 \times 2$  - spatial multiplexing) signal depending on SNR in the measured 60GHz indoor multipath channel

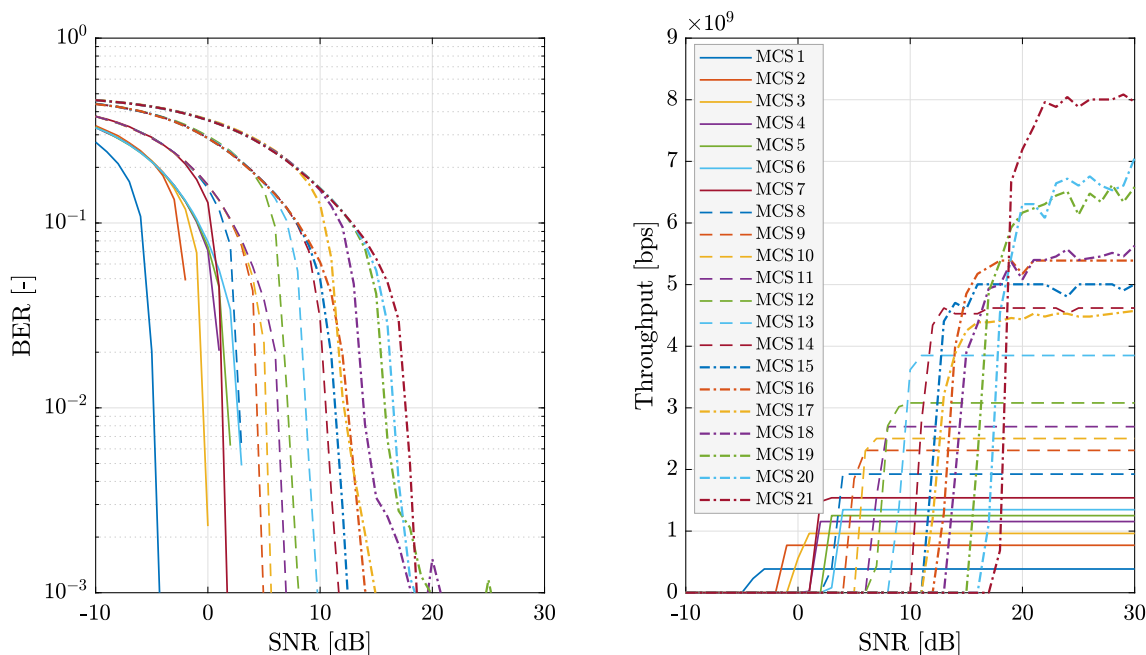
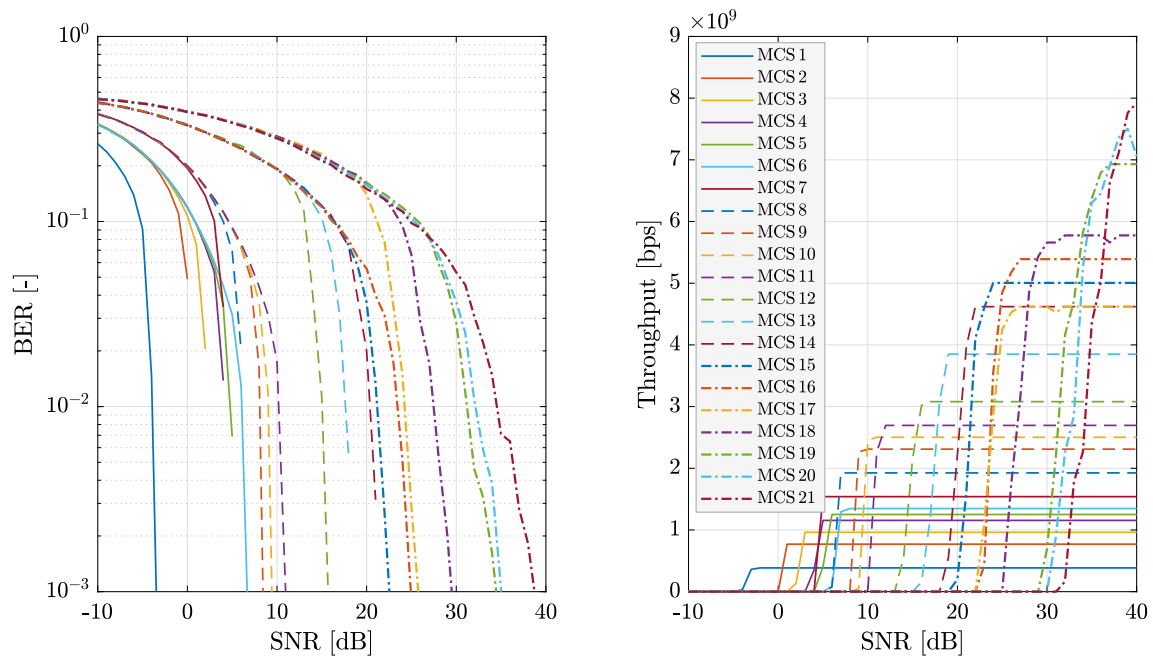


Fig. 13 BER and throughput curves of the 802.11ay SISO signal depending on SNR in the AWGN channel and at presence of PN

influence of PN. As is visible from Fig. 13, PN only has minor influence on the 802.11ay signal in the AWGN channel (see also Fig. 8).

The performance of uniform constellations (UCs) and NUCs in the 60GHz SISO channel in the presence of PN is shown in Figs. 14 and 15. As is briefly mentioned in [46], the NUCs, by optimizing the signal geometrical shaping, should

improve the immunity of the signal against RF impairments (e.g., PN) or fading for a specific channel model. The simulation results show minimal performance gain for NUCs (up to  $\approx 1$  dB), compared to scenarios in which ideal transmission conditions (AWGN) are assumed [47]. Such a lower NUC gain is probably caused by the features of the 60GHz indoor environment.



**Fig. 14** BER and throughput curves of the 802.11ay SISO signal depending on SNR in the measured 60GHz indoor multipath channel and at presence of PN. UCs are used for all MCS

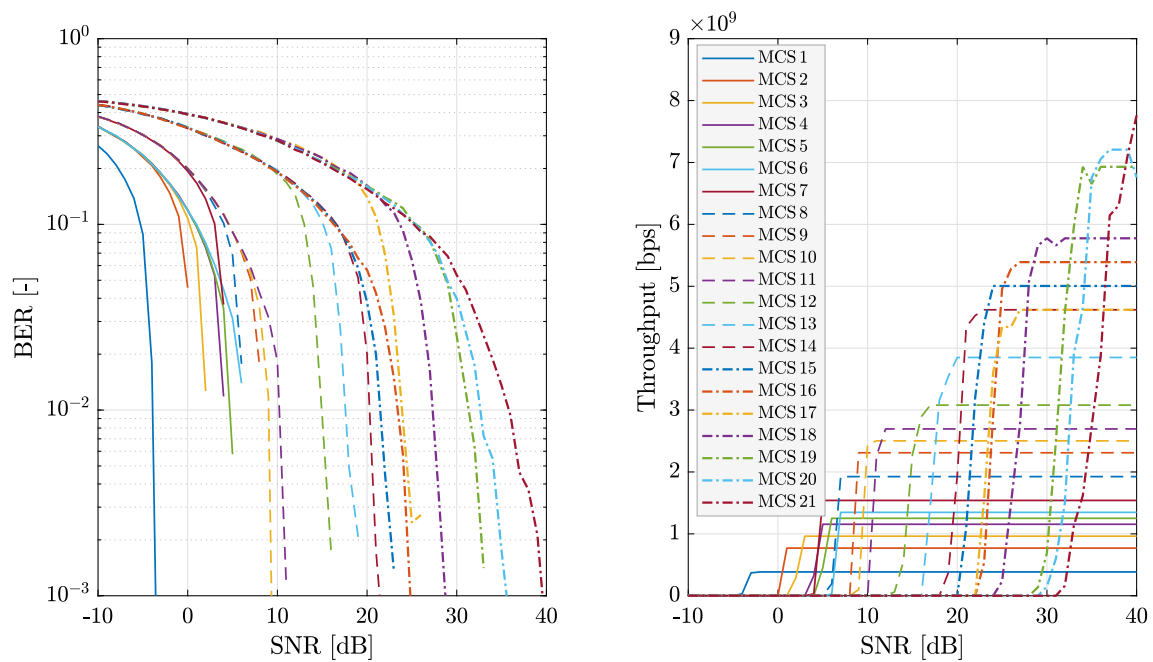


**Fig. 15** BER and throughput curves of the 802.11ay SISO signal depending on SNR in the measured 60GHz indoor multipath channel and at presence of PN. NUCs are used for MCS 18-21



## 5 Conclusion

This paper presented a simulation-based BER and throughput performance study of the IEEE 802.11ay SC-PHY system over measured 60 GHz indoor channels. For this purpose, a MATLAB-based baseband simulator with stable reproducibility was created and used. To support reproducible research, the introduced simulator as well as 60 GHz dataset are available under the MIT License for the research community at the project GitHub repository.<sup>4</sup>

As the simulation-based analyses shown, the MIMO scheme employing spatial multiplexing has positive influence on the data throughput dominantly in a transmission environment with strong AWGN features. On the other hand, utilizing of the SIMO transmission mode can offer stable BER and data throughput performance under 60 GHz indoor channel conditions. Next, it was shown that the 802.11ay SISO signal has good resistance against PN-based RF impairments. Finally, simulation results revealed only marginal improvement in the performance of the 802.11ay SISO signal when NUCs are utilized.

In the future, the study in this paper can be extended by the performance analysis of 802.11ay using OFDM-PHY layer. Next, the measured 60 GHz indoor channels dataset can be extended by other ones considering additional natures and conditions of an indoor environment (e.g., moving objects or interference caused by other system).

**Acknowledgements** This work was supported by the Ministry of Education, Youth and Sports (MEYS) of the Czech Republic project no. LTC18021 (FEWERCON).

**Author Contributions** All authors contributed to the study conception and design. Material preparation, data collection and analysis were performed by Ladislav Polak, Jiri Milos, Radim Zedka, Jiri Blumenstein and Christoph Mecklenbräuker. The first draft of the manuscript was written by Ladislav Polak and all authors commented on previous versions of the manuscript. All authors read and approved the final manuscript.

**Funding** The authors have not disclosed any funding.

## Declarations

**Conflict of interest** On behalf of all authors, the corresponding author states that there is no conflict of interest.

## References

1. Malik, A., Qadir, J., Ahmad, B., Yau, K. L. A., & Ullah, U. (2015). QoS in IEEE 802.11-based wireless networks: A contemporary review. *Journal of Network and Computer Applications*, 55, 24–46. <https://doi.org/10.1016/j.jnca.2015.04.016>.
2. Tripathi, P. S. M., & Prasad, R. (2018). Spectrum for 5G services. *Wireless Personal Communications*, 100(20), 540–555. <https://doi.org/10.1007/s11277-017-5217-9>.
3. Al-Falahy, N., & Alani, O. Y. (2019). Millimetre wave frequency band as a candidate spectrum for 5G network architecture: A survey. *Physical Communication*, 32, 120–144. <https://doi.org/10.1016/j.phycom.2018.11.003>.
4. Nitsche, T., Cordeiro, C., Flores, A. B., Knightly, E. W., Perahia, E., & Widmer, J. C. (2014). IEEE 802.11ad: Directional 60 GHz communication for multi-gigabit-per-second wi-fi. *IEEE Communications Magazine*, 52(12), 132–141. <https://doi.org/10.1109/MCOM.2014.6979964>.
5. Zhou, P., Cheng, K., Han, X., Fang, X., Fang, Y., He, R., et al. (2018). IEEE 802.11 ay-based mmwave WLANs: Design challenges and solutions. *IEEE Communications Surveys & Tutorials*, 20(3), 1654–1681. <https://doi.org/10.1109/COMST.2018.2816920>.
6. Abe, A., & Walker, S. D. (2016). Multi-hop 802.11 ad wireless H. 264 video streaming. In *2016 39th international conference on telecommunications and signal processing (TSP)* (pp. 94–99). IEEE. <https://doi.org/10.1109/TSP.2016.7760836>
7. Ghasempour, Y., da Silva, C. R., Cordeiro, C., & Knightly, E. W. (2017). IEEE 802.11 ay: Next-generation 60 GHz communication for 100 Gb/s Wi-Fi. *IEEE Communications Magazine*, 55(12), 186–192. <https://doi.org/10.1109/MCOM.2017.1700393>.
8. Eitan, A., Kasher, A., & Lomayev, A. (2018). *Technical change—64-QAM rate 1/2*. Technical report. IEEE
9. Rappaport, T. S., Heath, R. W., Jr., Daniels, R. C., & Murdock, J. N. (2015). *Millimeter wave wireless communications*. Pearson Education.
10. Zhu, X., Doufexi, A., & Kocak, T. (2011). Throughput and coverage performance for IEEE 802.11ad millimeter-wave WPANs. In *2011 IEEE 73rd vehicular technology conference (VTC Spring)* (pp. 1–5). IEEE. <https://doi.org/10.1109/VETECS.2011.5956194>
11. Zaaimia, M., Touhami, R., Hamza, A., & Yagoub, M. (2013). Design and performance evaluation of 802.11ad PHYs in 60 GHz multipath fading channel. In *2013 8th international workshop on systems, signal processing and their applications (WoSSPA)* (pp. 521–525). IEEE. <https://doi.org/10.1109/WoSSPA.2013.6602418>
12. Blumenstein, J., Milos, J., Polak, L., & Mecklenbräuker, C. (2019). IEEE 802.11ad SC-PHY layer simulator: Performance in real-world 60 GHz indoor channels. In *2019 IEEE Nordic circuits and systems conference (NorCAS)* (pp. 1–4). IEEE. <https://doi.org/10.1109/NORCHIP.2019.8906960>
13. Saha, S. K., Vira, V. V., Garg, A., & Koutsonikolas, D. (2016). A feasibility study of 60 GHz indoor WLANs. In *2016 25th international conference on computer communication and networks (ICCCN)* (pp. 1–9). IEEE. <https://doi.org/10.1109/ICCCN.2016.7568477>
14. Haider, M. K., & Knightly, E. W. (2016). Mobility resilience and overhead constrained adaptation in directional 60 GHz WLANs: Protocol design and system implementation. In *Proceedings of the 17th ACM international symposium on mobile ad hoc networking and computing* (pp. 61–70). ACM. <https://doi.org/10.1145/2942358.2942380>
15. Kacou, M., Guillet, V., El Zein, G., & Zaharia, G. (2018). Coverage and throughput analysis at 60 GHz for indoor WLANs with indirect paths. In *2018 IEEE 29th annual international symposium on personal, indoor and mobile radio communications (PIMRC)* (pp. 1–5). IEEE. <https://doi.org/10.1109/PIMRC.2018.8580903>
16. da Silva, C. R., Lomayev, A., Chen, C., Cordeiro, C. (2018). Analysis and simulation of the IEEE 802.11ay single-carrier PHY. In *2018 IEEE international conference on communications (ICC)* (pp. 1–6). IEEE. <https://doi.org/10.1109/ICC.2018.8422532>

<sup>4</sup> <https://github.com/jirimilos/802.11ay-phy-sim>.

17. Varshney, N., Zhang, J., Wang, J., Bodi, A., Golmie, N. (2020). Link-level abstraction of IEEE 802.11ay based on quasi-deterministic channel model from measurements. In *2020 IEEE 92nd vehicular technology conference (VTC2020-Fall)* (pp. 1–7). <https://doi.org/10.1109/VTC2020-Fall49728.2020.9348482>
18. Lei, L., Li, B., Yang, M., & Yan, Z. (2018). System analysis and performance evaluation for the next generation mmwave WLAN: IEEE 802.11ay. In *2018 IEEE international conference on signal processing, communications and computing (ICSPCC)* (pp. 1–6). IEEE. <https://doi.org/10.1109/ICSPCC.2018.8567616>
19. Assasa, H., Grosheva, N., Ropitault, T., Blandino, S., Golmie, N., & Widmer, J. (2021). Implementation and evaluation of a WLAN IEEE 802.11ay model in network simulator ns-3 (pp. 1–8).
20. Maltsev, A., Sadri, A., Cordeiro, C., & Puduev, A. (2015). Practical LOS MIMO technique for short-range millimeter-wave systems. In *2015 IEEE international conference on ubiquitous wireless broadband (ICUWB)* (pp. 1–6). IEEE. <https://doi.org/10.1109/ICUWB.2015.7324501>
21. Maltsev, A., Puduev, A., Lomayev, A., Bolotin, I. (2016) Channel modeling in the next generation mmwave wi-fi: IEEE 802.11ay standard. In *European wireless 2016; 22th European wireless conference* (pp. 1–8). VDE.
22. Lomayev, A., Gagiev, Y., Ershov, I., Maltsev, A., Genossar, M., & Bogdanov, M. (2016). Experimental investigation of 60 GHz wlan channel for office docking scenario. In *2016 10th European conference on antennas and propagation (EuCAP)* (pp. 1–5). IEEE. <https://doi.org/10.1109/EuCAP.2016.7481706>
23. Bodi, A., Zhang, J., Wang, J., Gentile, C. (2019). Physical-layer analysis of IEEE 802.11ay based on a fading channel model from mobile measurements. In *2019 IEEE international conference on communications (ICC 2019)* (pp. 1–7) (2019). <https://doi.org/10.1109/ICC.2019.8761887>
24. Pang, J., Maki, S., Kawai, S., Nagashima, N., Seo, Y., Dome, M., et al. (2019). A 50.1-Gb/s 60-GHz CMOS transceiver for IEEE 802.11ay with calibration of LO feedthrough and I/Q imbalance. *IEEE Journal of Solid-State Circuits*, 54(5), 1375–390. <https://doi.org/10.1109/JSSC.2018.2886338>.
25. Milos, J., Polak, L., & Slanina, M. (2017). Performance analysis of IEEE 802.11ac/ax WLAN technologies under the presence of CFO. In *2017 27th international conference radioelektronika (RADIOELEKTRONIKA)* (pp. 1–4). IEEE. <https://doi.org/10.1109/RADIOELEK.2017.7937579>
26. Milos, J., Polak, L., Hanus, S., & Kratochvil, T. (2017). Wi-Fi influence on LTE downlink data and control channel performance in shared frequency bands. *Radioengineering*, 26(1), 201–210. <https://doi.org/10.13164/re.2017.0201>.
27. Shadi, A. S., Josiam, K., Taori, R., & Chang, S. (2016). *Length 1344 LDPC codes for 11ay*. <https://mentor.ieee.org/802.11/dcn/16/11-16-0676-01-00ay-length-1344-ldpc-codes-for-11ay.pptx>
28. Xin, Y., Yan, M., Lin, W., Montorsi, G., & Benedetto, S. (2017). *Rate 7/8 (1344,1176) LDPC code*. <https://mentor.ieee.org/802.11/dcn/16/11-17-0069-01-00ay-rate-7-8-1344-1176-ldpc-code.pptx>
29. Lomayev, A., Maltsev, A., da Silva, C., Cordeiro, C., Genossar, M., Hansen, C., Lynch, B., Costa, N., Andonieh, J., Motozuka, H., & Sakamoto, T. (2017). *Vertical MIMO coding for SC and OFDM mode*. <https://mentor.ieee.org/802.11/dcn/17/11-17-1712-00-00ay-vertical-mimo-coding-for-sc-and-ofdm-mode.docx>
30. Al-Dhahir, N. (2017). Single-carrier frequency-domain equalization for space-time block-coded transmissions over frequency-selective fading channels. *IEEE Communications Letters*, 5(7), 304–306. <https://doi.org/10.1109/4234.935750>.
31. Schultz, B. (2013). *802.11 ad-WLAN at 60 GHz—A technology introduction*.
32. Eitan, A., Kasher, A., & Lomayev, A. (2018). *Technical change—64-QAM rate 1/2*. <https://mentor.ieee.org/802.11/dcn/11-18-0403-01-00ay-64-qam-rate-1-2.docx>
33. Polak, L., & Kratochvil, T. (2013). Exploring of the DVB-T/T2 performance in advanced mobile TV fading channels. In *2013 36th international conference on telecommunications and signal processing (TSP)* (pp. 768–772). IEEE. <https://doi.org/10.1109/TSP.2013.6614042>
34. Zeng, K., Cai, H., Wang, G., & Xin, Y. (2016). *Considerations on phase noise model for 802.11ay*. <https://mentor.ieee.org/802.11/dcn/16/11-16-0390-01-00ay-11ay-phase-noise-model.pptx>
35. Lomayev, A., Kravtsov, V., Genossar, M., Maltsev, A., & Khoryaev, A. (2020). Method for phase noise impact compensation in 60 GHz OFDM receivers. *Radioengineering*, 29(1), 159–173. <https://doi.org/10.13164/re.2020.0159>.
36. Yong, S. K., Xia, P., & Valdes-Garcia, A. (2011). *60 GHz technology for Gbps WLAN and WPAN: From theory to practice*. Hoboken: Wiley.
37. Liu, P., Blumenstein, J., Perović, N. S., Di Renzo, M., & Springer, A. (2018). Performance of generalized spatial modulation MIMO over measured 60 GHz indoor channels. *IEEE Transactions on Communications*, 66(1), 133–148. <https://doi.org/10.1109/TCOMM.2017.2754280>.
38. Chandra, A., Prokeš, A., Mikulášek, T., Blumenstein, J., Kukolev, P., Zemen, T., & Mecklenbräuker, C. F. (2016). Frequency-domain in-vehicle UWB channel modeling. *IEEE Transactions on Vehicular Technology*, 65(6), 3929–3940. <https://doi.org/10.1109/TVT.2016.2550626>.
39. Blumenstein, J., Vychodil, J., Pospisil, M., Mikulasek, T., Prokes, A. (2016). Effects of vehicle vibrations on mm-wave channel: Doppler spread and correlative channel sounding. In *IEEE 27th annual international symposium on personal, indoor, and mobile radio communications (PIMRC)* (pp. 432–437) (2016)
40. Xu, H., Kukshya, V., & Rappaport, T. (2002). Spatial and temporal characteristics of 60-GHz indoor channels. *IEEE Journal on Selected Areas in Communications*, 20(3), 620–630. <https://doi.org/10.1109/49.995521>.
41. Maltsev, A., Erceg, V., Perahia, E., Hansen, C., Maslennikov, R., Lomayev, A., Sevastyanov, A., & Khoryaev, A. (2009). *Conference room channel model for 60 GHz WLAN systems—Summary*. IEEE 802.11-09/0336r0.
42. Mehlführer, C., Wrulich, M., Ikuno, J. C., Bosanska, D., & Rupp, M. (2009). Simulating the long term evolution physical layer. In: 2009 17th European signal processing conference (pp. 1471–1478). IEEE.
43. Jaiyong, L., & Kang, C. (2003). *Mobile communications*. Springer.
44. Julius, M. S. (2016). MIMO: State of the art and the future in focus. <https://arxiv.org/abs/1610.05209>
45. Korhonen, J. (2014). *Introduction to 4G mobile communications*. Artech House
46. Feng, X. (2019). *Addressing test challenges of 802.11ay technology*. Keysight Technologies.
47. Handte, T., Ciochina, D., & Schneider, D. (2016). *Performance of non-uniform constellations in presence of phase noise*. <https://mentor.ieee.org/802.11/dcn/16/11-16-0072-00-00ay-performance-of-non-uniform-constellations-in-presence-of-phase-noise.pptx>

**Publisher's Note** Springer Nature remains neutral with regard to jurisdictional claims in published maps and institutional affiliations.



**Ladislav Polak** was born in Štúrovo, Slovakia in 1984. He received the M.Sc. degree in 2009 and the Ph.D. degree in 2013, both in Electronics and Communication from the Brno University of Technology (BUT), Czech Republic. He is currently an Associate Professor at the Department of Radio Electronic (DREL), BUT. His research interests are digital video broadcasting and wireless communication systems, RF measurement, signal processing and computer-aided analysis.



**Jiri Milos** was born in Uherské Hradiště, Czech Republic in 1986. He received his B.Sc. degree in Telecommunications in 2008, and M.Sc. and Ph.D. degrees in Electronics and Communication in 2010 and 2014, respectively, all from Brno University of Technology, Czech Republic. Currently, he is with the Department of Radio Electronics, Brno University of Technology, as a researcher. His research interests include wireless communication systems, modeling, digital signal processing,

rapid prototyping and RF measurement.



**Radim Zedka** received his B.Sc. degree in 2016, and M.Sc. degree in 2019 both in Electronics and Communication at Brno University of Technology (BUT). He is currently a PhD student at the Department of Radio Electronics of BUT and in his research activities he cooperates with Racom Ltd. on the development of mission-critical wireless communication systems. His main research interests are signal processing, physical layer of broadband wireless communication systems with focus on MIMO.

tems with focus on MIMO.



**Jiri Blumenstein** (M'17) received the Ph.D. degree from the Brno University of Technology, in 2013. In 2011, he was a Researcher with the Institute of Telecommunications, TU Wien. He has cooperated with several companies, including Racom, Volkswagen, and ON Semiconductor, in the areas of applied research of wireless systems and fundamental research funded by the Czech Science Foundation. He is currently a Researcher with the Department of Radio Electronics, Brno University of Technology. His research interests include signal processing, physical layer of communication systems, channel characterization and modeling, and wireless system design.

iversity of Technology. His research interests include signal processing, physical layer of communication systems, channel characterization and modeling, and wireless system design.



**Christoph Mecklenbräuer** (S'88-M'97-SM'08) received the Dipl. Ing. degree (Hons.) in electrical engineering from TU Wien, in 1992, and the Dr. Ing. degree (Hons.) from the Ruhr-Universität Bochum, Bochum, Germany, in 1998. From 1997 to 2000, he was with Siemens AG, Austria, where he was engaged in the standardization of the radio access network for UMTS. From 2000 to 2006, he was a Senior Researcher with the Telecommunications Research Center Vienna (FTW),

Vienna. In 2006, he joined the Institute of Communications and Radio Frequency Engineering, TU Wien, as a Full Professor. From 2009 to 2016, he led the Christian Doppler Laboratory for Wireless Technologies for Sustainable Mobility. He has authored approximately 250 papers in international journals and conferences, for which he has also served as a Reviewer. He holds several patents in the field of mobile cellular networks. His current research interests include radio interfaces for peer-to-peer networks (vehicular connectivity and sensor networks), ultra-wideband radio, and MIMO transceivers. He is also a member of the Antennas and Propagation Society, the Intelligent Transportation Society, the Vehicular Technology Society, the Signal Processing Society, VDE, and EURASIP. He is also the Councilor of the IEEE Student Branch Wien. His doctoral dissertation received the Gert-Massenberg Prize, in 1998.